Journal of Materials Processing Technology 231 (2016) 382–388

Contents lists available at ScienceDirect

Journal of Materials Processing Technology

journal homepage: www.elsevier.com/locate/jmatprotec

Dissimilar ultrasonic spot welding of aerospace aluminum alloy AA2139 to titanium alloy TiAl6V4

C.Q. Zhang[a,b,*], J.D. Robson[a], P.B. Prangnell[a]

[a] Materials Science Centre, School of Materials, University of Manchester, Grosvenor Street, Manchester M13 9PL, UK
[b] Shanghai Key Laboratory of Digital Manufacture for Thin-Walled Structures, School of Mechanical Engineering, Shanghai Jiao Tong University, Shanghai 200240, PR China

ARTICLE INFO

Article history:
Received 29 September 2015
Received in revised form 6 January 2016
Accepted 11 January 2016
Available online 19 January 2016

Keywords:
Dissimilar welding
Ultrasonic welding
Aluminum
Titanium
Intermetallic layer
Welding thermal cycle

ABSTRACT

The microstructure, hardness, lap shear strength and fracture energy of AA2139–TiAl6V4 spot joints produced by ultrasonic welding were investigated and related to the weld thermal cycle. No obvious intermetallic reaction layer was observed in the AA2139–TiAl6V4 welds, even using transmission electron microscopy. The hardness profile of AA2139 side after welding was studied, demonstrating that the heat introduced by the welding process leads to some softening with partial hardness recovery after natural aging. The effects of welding time on peak load and fracture energy were investigated. The peak load and fracture energy of welds increased with an increase in welding time and then reached a plateau, i.e., maximum peak load 5.3 kN and maximum fracture energy 3.7 kN mm. In all cases, failure occurred by fracture at the weld interface.

1. Introduction

Weight and cost reduction is a critical challenge in the aerospace industry so as to reduce fuel cost and enhance aircraft performance. Rendigs (1997) suggested that light-weight, lower cost design by replacing monolithic titanium components with multi-material parts produced from titanium and aluminum alloys is a promising route to achieve this objective.

This requires the joining of structures made of titanium alloys and aluminum alloys. Many investigations on Al/Ti joining have focused on fusion welding techniques, such as brazing, laser brazing and laser welding. Brittle intermetallic phases, typically Al_3Ti are often observed in these liquid-state welded Al/Ti joints, which can deteriorate the joint mechanical properties. For example, Chen et al. (2011b) welded Ti6Al4V titanium sheet and Al 5A06 sheet together by laser brazing with a filler wire made from aluminum alloy. Both $Ti_7Al_5Si_{12}$ and Al_3Ti phases were observed in the reaction layer. The thickness of the reaction layer varies from a few microns to around 50 μm depending on the welding parameters. Chen et al. (2011a) also found that compared with circular spot laser mode, rectangular spot laser with relative uniform energy distribution can enhance the uniformity of interfacial reaction along the interface. Chang et al. (2012) brazed 6061 aluminum alloy and Ti6Al4V using an Al–Si–Cu–Ge–Re filler metal, and an $Al_5Si_{12}Ti_7$ intermetallic compound (IMC) layer with a thickness of 3–6 μm was observed on the weld interface. (Peyre et al., 2014) laser lap welded Al (AA5754) and Ti (T40) using a Al–Si filler wire, and an IMC layer mainly composed of Al_3Ti with a thickness varying from 0.5 to 2.4 mm was observed on the weld interface. Tomashchuk et al. (2015) directly laser welded aluminum alloy AA5754 to titanium alloy Ti6Al4V without using any filler metal. TiAl, Al_3Ti and Ti_3Al intermetallic phases were detected in the weld by X-ray diffraction (XRD). Very recently, Casalino et al. (2015) also directly laser welded Al (AA5754) and Ti (T40) by offsetting the laser beam into the Ti side of the joint. Again, Al_3Ti intermetallic phase was observed on the weld interface. In summary, liquid-state dissimilar joining of aluminum to titanium is often accompanied by an obvious intermetallic layer formed on the Al/Ti interface. Such a layer, which is brittle compared to the parent materials, will degrade the performance on the joint.

Solid state welding processes are expected to suppress the IMC layer growth, due to their low energy input compared with fusion welding processes. Diffusion bonding, friction welding, friction stir welding (FSW) and friction spot welding have been used to weld

* Corresponding author at: Shanghai Key Laboratory of Digital Manufacture for Thin-Walled Structures, School of Mechanical Engineering, Shanghai Jiao Tong University, Shanghai 200240, PR China.
E-mail addresses: chaoqun.zhang@manchester.ac.uk, chaoqunzhang@sjtu.edu.cn (C.Q. Zhang).

http://dx.doi.org/10.1016/j.jmatprotec.2016.01.008

aluminum to titanium. However, intermetallic phases are still often observed on the interface. For example, Jiangwei et al. (2002) diffusion welded commercially pure Al and commercially pure Ti at 640 °C with a holding time of 90 min. Intermetallics AlTi and Al_3Ti were detected in the transition zone on the Ti side by XRD. Chen and Nakata (2009) have lap joined ADC12 cast aluminum alloy sheet and commercially pure titanium sheet by FSW. The maximum failure load of lap joints reached 62% that of the aluminum base metal. Al_3Ti phase was detected on the weld interface by XRD. Dressler et al. (2009) but welded 2 mm thick AA2024-T3 aluminum alloy and TiAl6V4 titanium alloy using FSW by shifting the tool pin toward the aluminum side. The joint ultimate tensile strength (348 MPa) reached 73% of the AA2024-T3 base material. Aonuma and Nakata (2011) also butt welded 2024-T3 and 7075-T651 aluminum alloy to pure titanium and Ti6Al4V alloy by FSW. The tool probe was also shifted to the aluminum side. In their joints, the highest average tensile strength reached 311 MPa. Al_3Ti intermetallic phase was again detected by XRD on the fracture surface of the weld. No other intermetallic compounds were detected. Besides Al_3Ti phase, Kimura et al. (2005) have observed $Ti_2Mg_3Al_{18}$ phase in a friction welded joint between an AlMg alloy (AA5052) and TiAl6V4. Plaine et al. (2015) lap joined 1.5 mm thick aluminum alloy AA6181-T4 and titanium alloy Ti6Al4V plates using friction spot welding technique. Sound joints with lap shear strength that can reach 6449 N were achieved.

High power ultrasonic spot welding (HP-USW) is a promising solid state welding process for joining thin metal sheets with very low energy input. Bakavos and Prangnell (2010) reported that the welding energy input of USW is very low, only around 2% of resistance spot welding—a fusion welding process, and ~30% of friction stir spot welding. It has been used for welding many dissimilar metal combinations, such as Al/Fe, Al/Mg, Al/Cu and Al/Ti. Although USWs have a low input energy, which is beneficial for suppressing IMC layer growth, when welding high-reactivity dissimilar metal combinations, an IMC layer is still typically formed at the interface. For example, Prangnell et al. (2011) observed an Al–Fe IMC layer (<2 μm) in USWed Al–Fe joints; Panteli et al. (2012) reported a fast growing Al–Mg IMC layer (up to 20 μm within 1 s welding time) in USWed Al–Mg joints; Yang and Cao (2015) observed an Al–Cu IMC layer (1–8 μm) in USWed Al–Cu joints. Recently, both the present authors Zhang et al. (2014) and Magin and Balle (2014) have reported that in Al/Ti joints (Al (AA6111 aluminum)/TiAl6V4 and AA1199/commercially pure titanium joints respectively) produced by USW, no visible IMC layer was detected on the weld interface even using high resolution transmission electron microscopy (TEM). The present authors Zhang et al. (2014) also have demonstrated that optimized USWed AA6111/Ti spot weld has an encouraging lap shear strength, which reached the same level as similar AA6111/AA6111 spot welds. The good mechanical properties compared with those of Al–Fe (Prangnell et al. (2011) and Al–Mg (Panteli et al. (2012) welds produced using the same technique is thought to be due to the lack of a thick brittle IMC layer at the interface. However, in the aerospace industry, 2XXX series aluminum alloys, rather than 1XXX series and 6XXX series, are most commonly used. Therefore, investigating the interfacial microstructure and the mechanical properties of 2XXX aluminum alloy/TiAl6V4 USW joint is important for the potential use of USW in aerospace industry.

In this study, the most frequently used aerospace titanium alloy (TiAl6V4) was joined to AA2139, a recently developed aerospace Al–Cu–Mg–Ag alloy. The objective of this work is not only to assess the suitability of HP-USW for joining high strength aerospace aluminum alloy to TiAl6V4, but also to investigate and evaluate the USWed joints from both mechanical and metallurgical points of view.

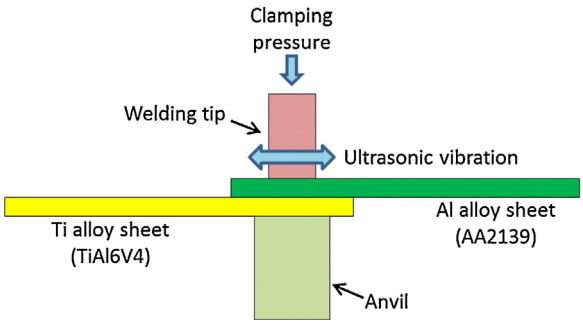

Fig. 1. Schematic diagram of the ultrasonic spot welding process.

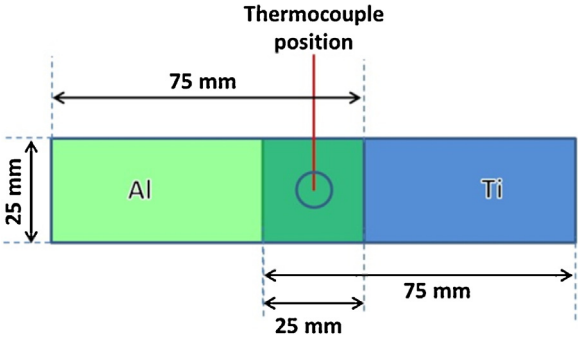

Fig. 2. Schematic diagram showing the position of the thermocouple.

2. Experimental methods

AA2139-T8 (Al–0.45Mg–0.03Si–4.8Cu–0.05Fe–0.3Mn–0.3Ag–0.0008Li) aluminum alloy and TiAl6V4 (Ti–6.15Al–4V–0.3Fe–0.1C–0.05N–0.015H–0.2O) titanium alloy sheets were used for the present study. Both of these materials are extensively used in the aerospace industry. The alloys were cut into 25 × 75 × 1 mm specimens and lap welded with aluminum sheet on the top, using a 2.5 kW single reed Sonobond ultrasonic welding machine, operating at 20.5 kHz. The welding time, which ranged from 0 s to 4 s, is the only variable parameter in this study. The welding energy is simply proportional to the welding time and has a maximum of approximately 4 kJ, as the weld power is kept constant. The pressure applied was also kept constant at 0.55 MPa. The sonotrode tip was of circular cross section with a diameter of 10 mm. It was aligned at the centre of a 25 mm overlap between the sheets when ultrasonic spot welding was performed. A schematic diagram of the typical single reed ultrasonic spot welding process is shown in Fig. 1. The sheet surfaces were ground using 300 grit grinding paper and then washed using acetone and dried prior to welding. To measure the thermal cycle during the welding process, 0.5 mm diameter k-type thermocouples were inserted into a groove between AA2139 sheet and TiAl6V4 sheet. The end of thermocouple is located at the centre of the clamped region, as illustrated in Fig. 2, and is expected to correspond to the maximum temperature position.

The mechanical properties of the joints were measured by tensile lap shear tests performed with a crosshead speed of 1 mm/min. The tensile lap shear tests were performed on the welded coupons without further machining. Specimens for lap shear testing were naturally aged for 8 days after welding to allow natural aging to occur close to completion. Hardness measurements were performed on metallographically polished surfaces across the welds at a depth of 0.5 mm below the top aluminum sheet surface using a Vickers microhardness testing machine with a load of 500 g.

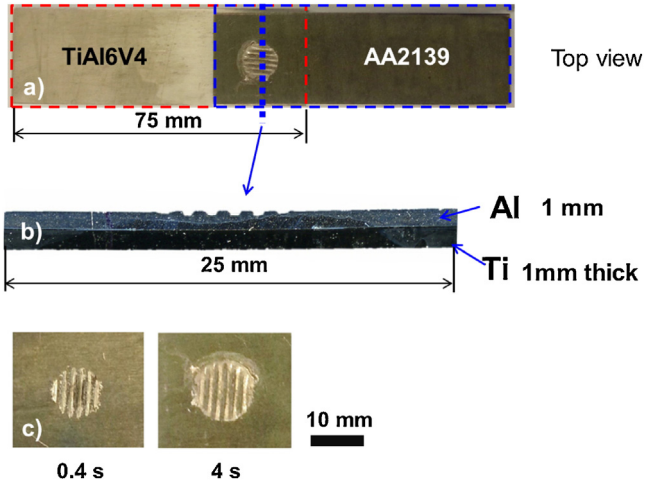

Fig. 3. (a) Weld appearance of a typical USW weld, welding time 4 s, welding energy 4120 J, (b) Macrostructure of cross-section of a typical USW weld, welding time 4.0 s, welding energy 4120 J, (c) Influence of welding time on welding tip indent area, sample photos (aluminum side).

The samples for microstructural investigations were cross-sectioned perpendicular to the welding direction, which is parallel to the ultrasonic vibration direction, and prepared for metallographic investigation using standard methods. The microstructure near the interface was observed with back-scattered electrons using an FEI Quanta 650 field emission scanning electron microscopy (FE-SEM) equipped with an energy-dispersive X-ray spectroscopy (EDS) detector.

Thin foils for transmission electron microscopy (TEM) were prepared by Focused Ion Beam Milling (FIB) using a FEI QUANTA 3D FIB system operating at 30 kV for rough cutting and milling, and both 5 kV and 2 kV for final cleaning. The foils were examined using a Tecnai TF30 transmission electron microscope operating at 300 kV.

3. Results and discussion

3.1. Weld appearance

Fig. 3(a) shows the appearance of a typical Al–Ti (AA2139–TiAl6V4) dissimilar weld (welding time 4.0 s, welding energy 4120 J) produced by USW. The macrostructure of cross-section of a USW joint is shown in Fig. 3(b). It can be seen that AA2139 aluminum alloy sheet was severely deformed by the welding tip and there was almost no macro deformation on the titanium side. The reason for this is discussed later in the weld microstructure section.

Fig. 3(c) shows surface appearances of AA2139/Ti6Al4V joints for different welding times. It can be seen that the indent area

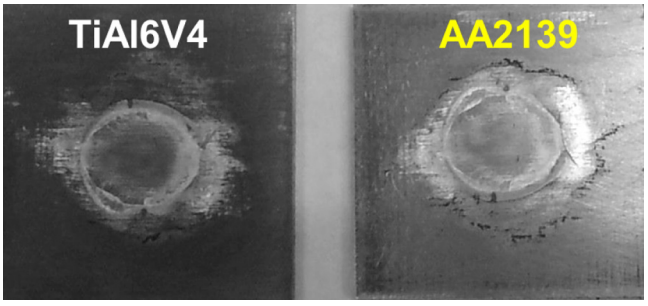

Fig. 5. The 'interfacial failure' mode of AA2139/TiAl6V4.

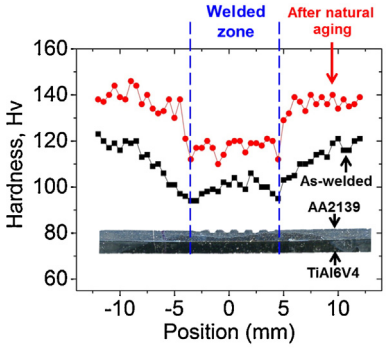

Fig. 6. Hardness profile across the aluminum alloy in AA2139/TiAl6V4 weld (4 s, 4250 J) measured 30 min (square markers) and 8 days (circular markers) after welding. (Hardness test load: 500 g, dwell time: 10 s).

increased with increasing welding time, due to the softening of AA2139 aluminum alloy and the downward movement of the welding tip with increasing welding time.

3.2. Mechanical properties

3.2.1. Effect of welding time

In this study, the welding time is the only variable welding parameter. Since the weld power remained unchanged, an increase in weld time also corresponds to an increase in total energy input into the weld.

As shown in Fig. 4(a), the peak load that can be sustained before failure of the Al–Ti weld increased with an increase of welding time from 0 s to 2.0 s. For times longer than this, peak load plateaus, with an upper limit around 5.3 kN (~100 MPa, shear strength). This peak load is much higher than that measured during testing of optimized Al–Mg (Panteli et al., 2012) USW welds (~2.0 kN) and Al–Fe (Prangnell et al., 2011) USW welds (~2.8 kN) of similar dimensions. This is mainly due to the very limited interfacial reaction between Al and Ti (as discussed later in Section 3.3) compared with the

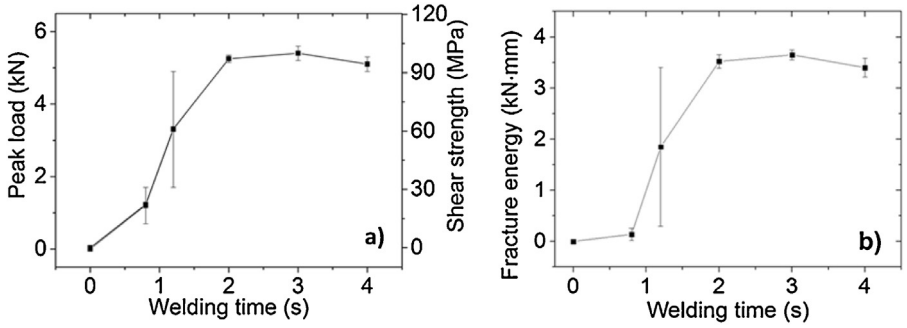

Fig. 4. (a) Effect of welding time on the peak load and shear strength of AA2139/TiAl6V4 USW welds; (b) Effect of welding time on fracture energy of AA2139/TiAl6V4 welds.

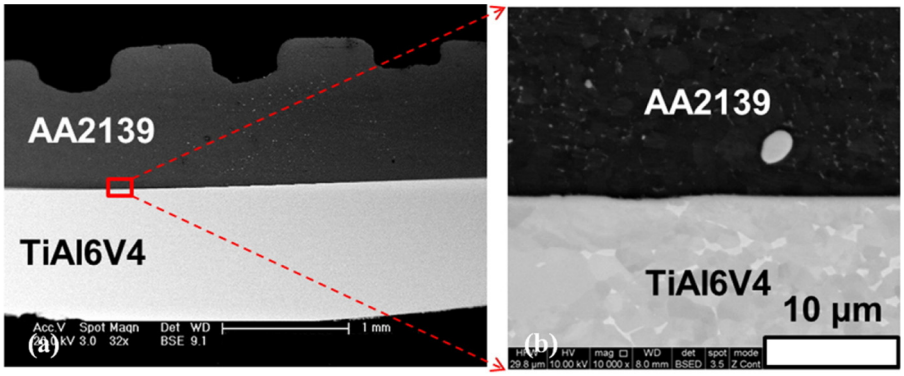

Fig. 7. SEM images of typical AA2139–TiAl6V4 ultrasonic spot weld interface (welding time: 4 s, welding energy: 4120 J) (a) low magnification image, (b) high magnification BSE image.

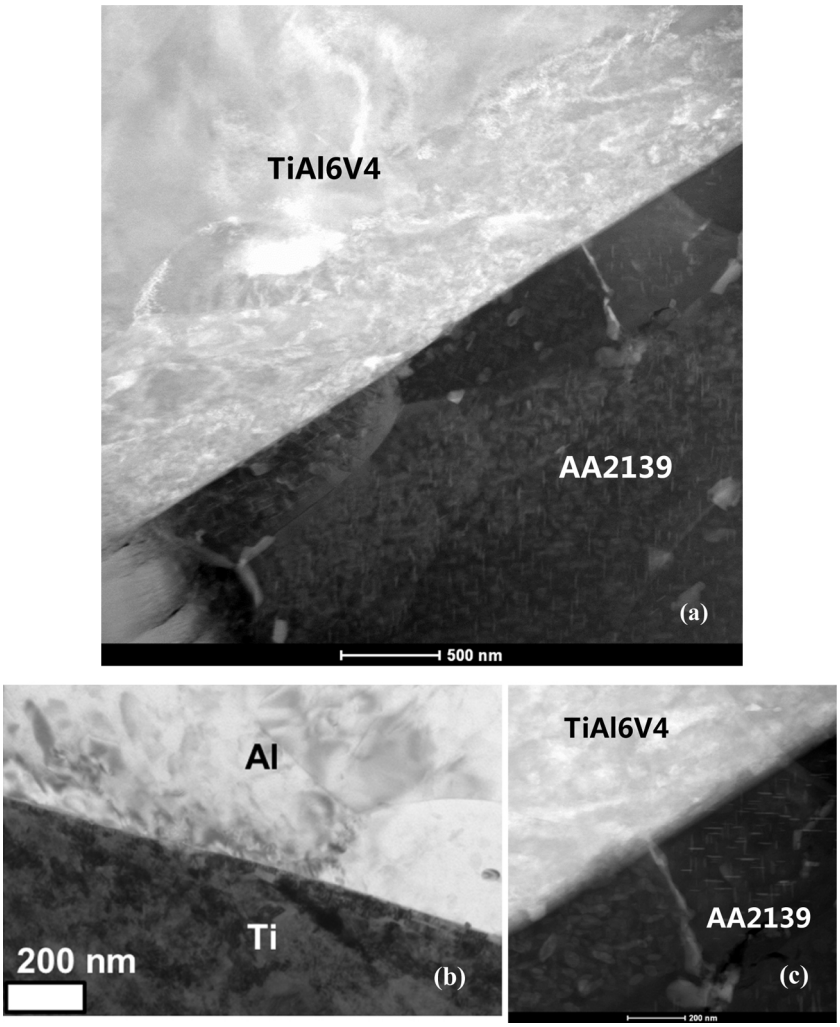

Fig. 8. TEM images of an AA2139–TiAl6V4 USW weld interface, (a) a low magnification HAADF image showing a large region of the interface, (b) higher magnification bright field image, (c) higher magnification HAADF image, (welding time: 4.0 s, welding energy: 4120 J).

rapid interfacial reaction in Al–Mg welds and Al–Fe welds, which is discussed in more detail elsewhere (Zhang et al., 2014).

The highest peak load reached is also higher than (~51%) that of optimized AA6111–TiAl6V4 USW welds (~3.5 kN) (Zhang et al., 2014), which shared a similar interfacial failure mode (discussed later). This can be largely attributable to the increased area of the welding tool used in the present study (tool cross-section area: 79 mm^2, ~46% larger) compared with that used for welding AA6111/TiAl6V4 (Zhang et al., 2014). A larger welding tool leads to a larger welded area and thus increased failure load.

The high degree of scatter in the peak loads for the joints made using welding time 1.2 s is because this time corresponds to the transition between the partially bonded (short welding time) and fully bonded conditions (long welding time, >2.0 s). As shown in Fig. 4, for welding times shorter than 0.8 s, almost no weld can form; for welds longer than 2 s, a fully bonded weld always forms. In gen-

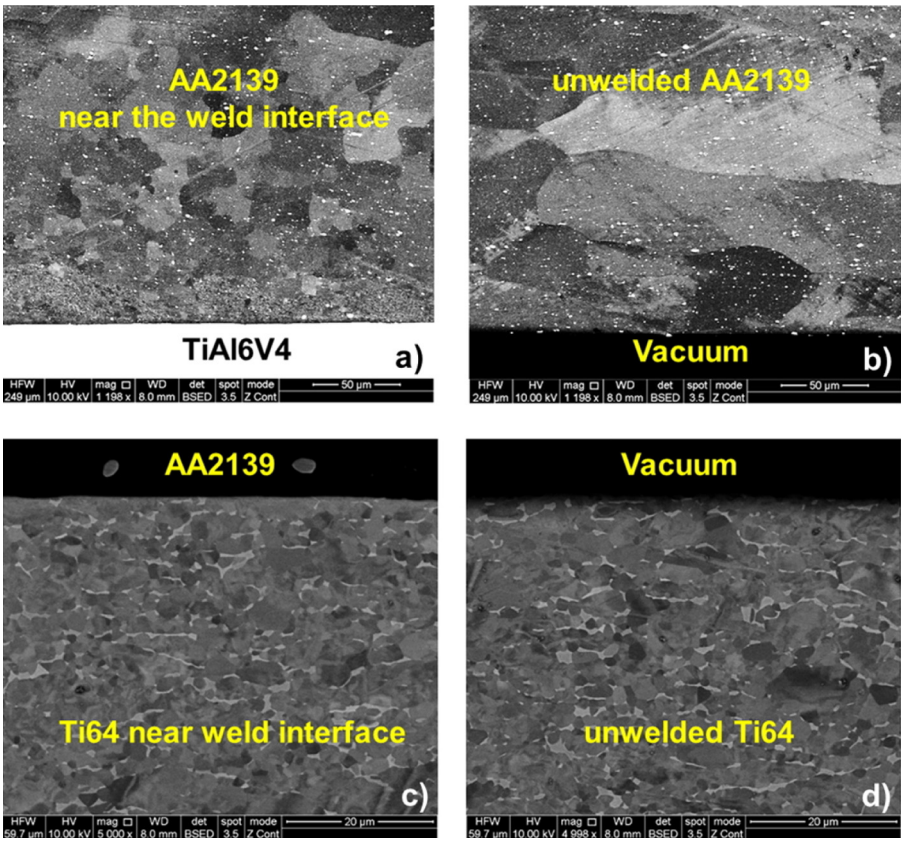

Fig. 9. Comparison of microstructure between aluminum alloy AA2139 near the weld interface ((a), welding time 3.0 s) and AA2139 base metal near surface region ((b), not welded); Comparison of microstructure between TiAl6V4 near the weld interface ((c), welding time 3.0 s) and not-welded TiAl6V4 base metal near surface region ((d), not welded).

eral, the welding time—peak load relationship of AA2139–TiAl6V4 welds is quite similar to that of AA6111–TiAl6V4 welds (Zhang et al., 2014), with peak load initially increasing with increasing welding time before reaching a plateau.

As shown in Fig. 4(b), the variation trend of fracture energy with increasing welding time is similar with the trend of peak load (Fig. 4(a)). The fracture energy reached an upper limit around 3.7 kN mm when the welding time is longer than 2 s.

As Fig. 5 shows, weld failure at all weld times was observed to occur by fracture across the interface, and no aluminum remained stuck on the titanium sheet after testing. This is in contrast to USW AA6111–TiAl6V4 joints, where a nugget pull out condition could be achieved which was accompanied by extensive deformation of aluminum leading to a high fracture energy (Zhang et al., 2014). This difference is due to the higher strength of AA2139 alloy compared with the AA6111 alloy, which means that interfacial failure occurs before significant plastic deformation of the aluminum alloy.

Though the optimized AA2139–TiAl6V4 USW weld peak load (~5.3 kN) is 51% higher than that of AA6111–TiAl6V4 USW weld (~3.5 kN) (Zhang et al., 2014), the optimized AA2139–TiAl6V4 USW weld fracture energy (~3.7 kN mm) is 26% lower than that of AA6111–TiAl6V4 USW weld (~5 kN mm, naturally aged) (Zhang et al., 2014). This is consistent with the interfacial failure mode always observed for the AA2139–TiAl6V4 welds as already noted.

3.2.2. Hardness profile

Fig. 6 shows the hardness profile in the AA2139 aluminum alloy close to the interface along the weld, measured within 30 min of welding and after 8 days natural aging. It can be seen that similar to other solid state welding processes, such as friction stir welding (Jata et al., 2000), the USW process has led to a significant (approximately 37%) softening of the aluminum alloy in the weld zone and the heat affected zone, due to the dissolution and coarsening of the strengthening precipitates (Jata et al., 2000). After 8 days natural aging, the hardness recovered partly, because of the re-precipitation of the alloying elements dissolved during the welding process. In contrast to the AA6111–TiAl6V4 USW joints (Zhang et al., 2014), the strength recovery of AA2139 did not lead to the change of failure mode of the AA2139–TiAl6V4 USW welds since even in the "as welded" (soft) condition, the AA2139 alloy is strong enough to produce an interfacial failure mode in the weld.

3.3. Weld microstructure

Fig. 7(a) and (b) shows a typical AA2139–TiAl6V4 weld microstructure (cross section), for a 4 s welding time joint. No IMC layer was visible in these AA2139/TiAl6V4 weld backscattered electron images even at the highest magnifications, which is encouraging since the formation of a brittle IMC layer is typically associated with poor mechanical properties.

To investigate the weld interface at higher resolution, TEM was used. To make a careful study of the Al–Ti interface, both bright field images and high-angle annular dark field images (HAADF) were taken of the interface region with examples of these images shown in Fig. 8. Even using the higher resolution of the TEM, no obvious IMC layer was detected, suggesting if any layer is present it must be very thin (< 100 nm). Although atypical, similar "clean" (no-IMC-layer) interface structures have been noticed previously for other material combinations joined by ultrasonic welding and other approaches; for example, in the metal–metal case (Kim et al., 2014), metal–ceramic case (Matsunaga et al., 2006), and metal–glass combination (Iwamoto 2014). These no-IMC-layer

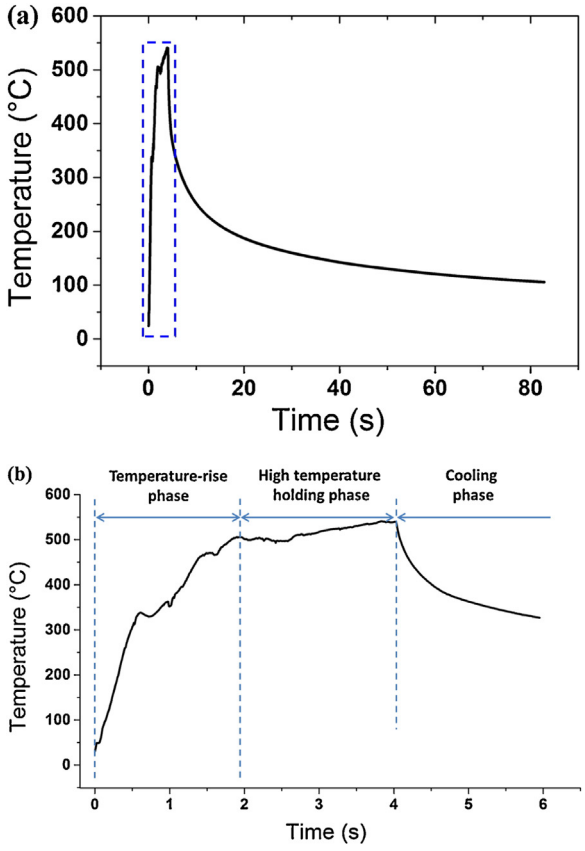

Fig. 10. Welding thermal cycle, (a) the total cycle of a 4.0 s welding time measured in the middle of the AA2139–TiAl6V4 weld, (b) the partial thermal cycles of the 4.0 s weld near the peak temperature region which is indicated by the blue rectangular in (a).

interfaces are typically associated with a very low welding energy or very high-energy barrier for nucleation of the IMC. Previous studies by both the present authors Zhang et al. (2014) and Magin and Balle (2014) on ultrasonic welding of Al and Ti also reported no reaction layer visible at the interface. In this case, a prolonged post-weld heat treatment (e.g., 5 h at 500 °C) is required to form detectable IMC layer.

The microstructure of AA2139 near the weld interface and the microstructure of unwelded AA2139 base metal in the near surface region at the same magnification are shown in Fig. 9(a) and (b). It can be seen that the Al grains near the weld interface have been refined by the USW process, which has also been found in other investigations on Al–Al and Al–Fe USW by Bakavos and Prangnell (2010) and Prangnell et al. (2011).

The microstructure of TiAl6V4 near the weld interface and the microstructure of unwelded TiAl6V4 base metal in the near-surface region at the same magnification are shown in Fig. 9(c) and (d). No apparent difference between the microstructure of the titanium alloy close to and far from the interface can be noticed. This suggests that little deformation occurred on the TiAl6V4 side near the weld interface, which might be expected due to the much higher strength of TiAl6V4 at the peak temperature reached during welding (approximately 540 °C, as discussed in detail later). Similar phenomena were also reported previously for dissimilar Al to steel USWs by Prangnell et al. (2011).

3.4. Welding thermal cycle

Fig. 10(a) shows a typical thermal profile for a 4.0 s weld measured at the centre of the weld as described in Section 2. To show more detail, the thermal cycle profile indicated in the blue rectangular region in Fig. 10(a) was enlarged and is shown in Fig. 10(b).

Similar to the ultrasonic welding thermal cycle of AA6111/TiAl6V4 (Zhang et al., 2014) joints, the welding thermal cycle of AA2139/TiAl6V4 can be divided into three phases: 1. Temperature-rise phase; 2. High temperature holding phase; 3. Cooling phase.

The long "temperature-rise phase" (~2.0 s) of AA2139/TiAl6V4 weld led to poor bonding in welds produced using welding times shorter than 2 s. The temperature at welding times <2 s is not high enough for sufficient inter-diffusion between AA2139 and TiAl6V4 to form a fully bonded weld. This is consistent with the poor mechanical properties measured for such short time welds. Successful joining of dissimilar metals (Al and Ti) highly depends on the degree of inter-diffusion between Al and Ti. When the inter-diffusion is sufficient, a diffusion zone or an IMC layer forms on the interface, which is necessary for forming a sound dissimilar metal weld. The "temperature-rise phase" (~2.0 s) of AA2139/TiAl6V4 weld is much longer compared with that of AA6111/TiAl6V4 weld (~0.4 s) (Zhang et al., 2014), as a result, it took longer time to form a sound joint for the AA2139/TiAl6V4 combination than for the AA6111/TiAl6V4 combination.

4. Conclusions

The feasibility of HP-USW for welding high strength aerospace aluminum alloy AA2139 to titanium alloy was studied. According to the present microstructural, mechanical property and welding thermal cycle investigation, the following conclusions were reached:

1. 1 mm thick AA2139 aluminum alloy sheet and 1 mm thick TiAl6V4 sheet can be successfully welded by high power ultrasonic spot welding.
2. The peak failure load of AA2139–TiAl6V4 welds in a lap shear test reached 5.3 kN (~100 MPa, shear strength). The excellent strength of Al–Ti joints compared to that of other dissimilar combinations, e.g., Al–Mg and Al–Fe is attributed to the lack of formation of brittle intermetallic in the Al–Ti case.
3. All the AA2139–TiAl6V4 welds show an 'interfacial failure' mode and have a low fracture energy. The 2139 aluminum alloy is sufficiently strong that it does not extensively plastically deform before the critical stress for interfacial failure is reached.
4. No obvious IMC layer was detected in AA2139/TiAl6V4 USW joints by scanning and transmission electron microscopy.
5. The peak welding temperature reached 540 °C and the time taken to reach this peak temperature was around 2 s.

Acknowledgements

This work was funded by the EPSRC through LATEST2, Light Alloys Towards Environmentally Sustainable Transport (EP/G022402/1) and Friction Joining—Low Energy Manufacturing for Hybrid Structures in Fuel Efficient Transport Applications (EP/G022402/1.JLR). The authors acknowledge the China Scholarship Council (CSC, 2011612001) for financial support and would like to thank Constellium and Airbus UK for the provision of materials.

References

Aonuma, M., Nakata, K., 2011. Dissimilar metal joining of 2024 and 7075 aluminium alloys to titanium alloys by friction stir welding. Mater. Trans. 52, 948–952.

Bakavos, D., Prangnell, P.B., 2010. Mechanisms of joint and microstructure formation in high power ultrasonic spot welding 6111 aluminium automotive

sheet. Mater. Sci. Eng. A: Struct. Mater. Properties Microstruct. Process. 527, 6320–6334.
Casalino, G., Mortello, M., Peyre, P., 2015. Yb–YAG laser offset welding of AA5754 and T40 butt joint. J. Mater. Process. Technol. 223, 139–149.
Chang, S.Y., Tsao, L.C., Lei, Y.H., Mao, S.M., Huang, C.H., 2012. Brazing of 6061 aluminum alloy/Ti–6Al–4V using Al–Si–Cu–Ge filler metals. J. Mater. Process. Technol. 212, 8–14.
Chen, S., Li, L., Chen, Y., Dai, J., Huang, J., 2011a. Improving interfacial reaction nonhomogeneity during laser welding-brazing aluminum to titanium. Mater. Des. 32, 4408–4416.
Chen, S., Li, L., Chen, Y., Huang, J., 2011b. Joining mechanism of Ti/Al dissimilar alloys during laser welding-brazing process. J. Alloys Compd. 509, 891–898.
Chen, Y.C., Nakata, K., 2009. Effect of tool geometry on microstructure and mechanical properties of friction stir lap welded magnesium alloy and steel. Mater. Des. 30, 3913–3919.
Dressler, U., Biallas, G., Alfaro Mercado, U., 2009. Friction stir welding of titanium alloy TiAl6V4 to aluminium alloy AA2024-T3. Mater. Sci. Eng. A 526, 113–117.
Iwamoto, C., 2014. Microstructure of aluminum/glass joint bonded by ultrasonic wire welding. Metall. Mater. Trans. A: Phys. Metall. Mater. Sci. 45A, 1371–1375.
Jata, K.V., Sankaran, K.K., Ruschau, J.J., 2000. Friction-stir welding effects on microstructure and fatigue of aluminum alloy 7050-T7451. Metall. Mater. Trans. A: Phys. Metall. Mater. Sci. 31, 2181–2192.
Jiangwei, R., Yajiang, L., Tao, F., 2002. Microstructure characteristics in the interface zone of Ti/Al diffusion bonding. Mater. Lett. 56, 647–652.
Kim, H.G., Kim, S.M., Lee, J.Y., Choi, M.R., Choe, S.H., Kim, K.H., Ryu, J.S., Kim, S., Han, S.Z., Kim, W.Y., Lim, S.H., 2014. Microstructural evaluation of interfacial intermetallic compounds in Cu wire bonding with Al and Au pads. Acta Mater. 64, 356–366.
Kimura, M., Nakamura, S., Kusaka, M., Seo, K., Fuji, A., 2005. Mechanical properties of friction welded joint between Ti–6Al–4V alloy and Al–Mg alloy (AA5052). Sci. Technol. Weld. Join. 10, 666–672.
Magin, J., Balle, F., 2014. Solid state joining of aluminum, titanium and their hybrids by ultrasonic torsion welding. Materialwiss. Werkstofftech. 45, 1072–1083.
Matsunaga, K., Sasaki, T., Shibata, N., Mizoguchi, T., Yamamoto, T., Ikuhara, Y., 2006. Bonding nature of metal/oxide incoherent interfaces by first-principles calculations. Phys. Rev. B 74.
Panteli, A., Robson, J.D., Brough, I., Prangnell, P.B., 2012. The effect of high strain rate deformation on intermetallic reaction during ultrasonic welding aluminium to magnesium. Mater. Sci. Eng.: A 556, 31–42.
Peyre, P., Berthe, L., Dal, M., Pouzet, S., Sallamand, P., Tomashchuk, I., 2014. Generation and characterization of T40/A5754 interfaces with lasers. J. Mater. Process. Technol. 214, 1946–1953.
Plaine, A.H., Gonzalez, A.R., Suhuddin, U.F.H., dos Santos, J.F., Alcântara, N.G., 2015. The optimization of friction spot welding process parameters in AA6181-T4 and Ti6Al4V dissimilar joints. Mater. Des. 83, 36–41.
Prangnell, P., Haddadi, F., Chen, Y.C., 2011. Ultrasonic spot welding of aluminium to steel for automotive applications—microstructure and optimisation. Mater. Sci. Technol. 27, 617–624.
Rendigs, K.H., 1997. Aluminium structures used in aerospace—status and prospects. In: Driver, J.H., Dubost, B., Durand, F., Fougeres, R., Guyot, P., Sainfort, P., Suery, M. (Eds.), Aluminium Alloys: Their Physical and Mechanical Properties, Part 4/Supplement. , pp. 11–23.
Tomashchuk, I., Sallamand, P., Cicala, E., Peyre, P., Grevey, D., 2015. Direct keyhole laser welding of aluminum alloy AA5754 to titanium alloy Ti6Al4V. J. Mater. Process. Technol. 217, 96–104.
Yang, J., Cao, B., 2015. Investigation of resistance heat assisted ultrasonic welding of 6061 aluminum alloys to pure copper. Mater. Des. 74, 19–24.
Zhang, C.Q., Robson, J.D., Ciuca, O., Prangnell, P.B., 2014. Microstructural characterization and mechanical properties of high power ultrasonic spot welded aluminum alloy AA6111–TiAl6V4 dissimilar joints. Mater. Charact. 97, 83–91.